Global Urban Heat Island Mitigation

Edited by
Ansar Khan
Hashem Akbari
Francesco Fiorito
Sk Mithun
Dev Niyogi

ELSEVIER

CHAPTER

Visualization of landuse change pattern and its impact on Urban Heat Islands

14

G. Nimish[1], H.A. Bharath[1] and T.V. Ramachandra[2]

[1]*Ranbir and Chitra Gupta School of Infrastructure Design and Management, Indian Institute of Technology Kharagpur, Kharagpur, West Bengal, India;* [2]*Centre for Ecological Science, Indian Institute of Science, Bangalore, Karnataka, India*

1. Introduction

It has been witnessed since the beginning of history, that humans have a tendency to prove themselves to be superior to all other living organisms. It is now truthful to state that there exists an ego among the human breed to dominate the available resources for their immediate benefits. Previously, this was just altering the local climate which was almost negligible as nature has a self-cleansing and maintaining property, but from past few decades, due to extreme pressure on nature, the climate across the globe is being affected due to anthropogenic activities. Initially, climate change was considered essential only on academic basis, but over the past few years, due to increased awareness among people, it has become one of the most concerned and researched topics, also being one of the most significant developmental challenges for humans (Lal, 2017). One of the most critical factors of changing climate can be inferred as unplanned and hap-hazardous urban areas development. Urbanization has conveniently brought numerous positive changes such as making cities economically sustainable, increasing the GDP per capita, providing a better standard of living and quality of life, improved medical facilities, increased occupational opportunities, and better education (Keeling, 1997; Karoly et al., 2003; Stott et al., 2006). However, due to increased demographic pressure on the cities due to large movement of population from rural to urban areas, rapid and unorganized developments have started to come-up in cities for satisfying the needs of incoming residents. These changes gradually collapse the balance, creating problems such as unavailability of basic housing, lack of fresh and treated water supply, inadequate infrastructure, and rise in greenhouse gases as well as pollution levels (Ramachandra et al., 2012). Scientific communications have found that these alterations in urban areas can be understood by deriving land use/land cover maps, and these maps can be used to demonstrate the phenomenon of urbanization. These changes in LULC includes the development of urban pockets (pervious surface) on the cost of areas that serves important feeders for human life such as vegetation, open/bare fields, agricultural fields, etc. (Kandlikar and Sagar, 1999; Mallick et al., 2008; Ramachandra et al., 2016). In today's scenario, there have been numerous cases where urban areas have come-up by encroaching water bodies such as lakes, ponds, and catchment areas, leading to a rise in urban floods. These unprecedented alterations in LULC affect evapotranspiration rates, surface

Global Urban Heat Island Mitigation. https://doi.org/10.1016/B978-0-323-85539-6.00001-9

albedo, storage of heat and moisture content of the surfaces, pollution displacement, and surface temperature (Pal and Ziaul, 2017). Due to such changes, the phenomenon of global warming has been intensifying over the years, and it creates a massive threat for sensitive species in nature as most of the flora and fauna are sensitive to temperature.

Researchers across the globe have found a strong relationship between alteration in LULC and climate change in terms of Land Surface Temperature (LST) (Aggarwal et al., 2012; Mutiibwa et al., 2014). LST is an important parameter that accounts for the upward thermal radiation and can be defined as the radiative skin temperature of the earth's surface. It is a crucial parameter to describe the thermal comfortability of the residents (Bento et al., 2017). LST not only affects human but also disturbs rainfall patterns, wind turbulence and speed, crop patterns, ecology of the region, and earth's natural cycles including biogeochemical cycle, water cycle, and carbon cycle. It is one of the key input parameters in numerous applications such as urban climatology, greenhouse gas quantification, crop monitoring, studies related to global warming and also defines the phenomena of Urban Heat Island (UHI) (Schmugge and Becker, 1991; Li and Becker, 1993; Running et al., 1994; Anderson et al., 2008; Li et al., 2013; Ramachandra et al., 2017; Khandelwal et al., 2018). UHI is a phenomenon that is being observed in many cities across the globe as a result of higher temperatures in urban areas when compared to nearby rural areas due to increased impervious surfaces in urban areas. UHI is an issue of serious concern as it is responsible for a large number of health-related issues and deaths across the globe. Thus, it is a need-of-hour to study the dreadful effects of rising LST on the inhabitants and suggest some mitigation measures.

Remote Sensing (RS) and Geographic Information System (GIS) have developed across the years and are now considered as a state-of-the-art technology for any climate and urban-related studies. Thus, the case study presented in this chapter uses remote sensing data and open source GIS software for complete analysis. This book chapter deals with the understanding of how changes in landscape due to increased anthropogenic activities affect climate in terms of land surface temperature. The chapter also deals with explaining how a rise in LST causes an increase in UHI effect, that further affects the health and welfare of inhabitants in an urban area with a case study. Also, few mitigation measures were suggested to reduce the overall rise and eliminate the ill-effects of LST. The chapter is divided into sections as mentioned below:

1. **Introduction:** This section gives a brief idea about the overall research work presented in this chapter.
2. **Understanding LST:** This section provides basic information about Land Surface Temperature.
3. **Urban Heat Islands**: This section deals with understanding the phenomenon of UHI.
4. **Significance of studying LST and UHI:** As the name suggests this chapter highlights the need and motivation behind studying LST and understanding the phenomenon of UHI in an urban area.
5. **Theoretical Background:** This section gives a brief introduction to the principles on which thermal remote sensing works.
6. **Practical example:** This section provides a case study showing a relationship between growing urban area and rise in LST, followed by the UHI index for Kolkata Metropolitan Area in India.
7. **Mitigation measures:** The section suggests a few mitigation measures that can be implemented for reducing the overall regional scale LST.
8. **Conclusion:** This section includes the takeaway points from this chapter.

2. Understanding LST

Land Surface Temperature is a direction-based radiometric temperature of the collective surfaces on the earth as observed from the thermal region of the sensor onboard (Sismanidis et al., 2016). It is a basic element of earth's thermal behavior and is an important index that determines the earth's energy balance and climate change (AATSR and SLSTR, 2018). It is an important indicator of global warming and greenhouse effect (Jia et al., 2007) and is directly linked with the sensible and latent heat fluxes, thus, playing a pivotal role in defining local, regional, as well as global processes over the surface of the earth (Mannstein, 1987). One of the main advantages of estimating LST is that it provides the value of temperature at a pixel level, thus making it possible to capture and map even a very minute change in temperature which is not possible with measurements collected from meteorological stations especially in case of developing countries as they have only one meteorological station installed for a large area. Changes in landscape affect the overall evaporation and transpiration rates that alter the latent and sensible heat fluxes (Mojolaoluwa et al., 2018). Scientific community across the globe have predicted that there would be higher climatic variation and increased thermal discomfort to the urban residents as a result of continuous rise in urban population because this will lead to increase in construction activities, rise in traffic congestions, and higher production of power supply. Fulfilling these needs would hamper the environment critically as they will lead to an increment in the concentration of pollutants in the air (PM_{10}, $PM_{2.5}$, PM_1, and Suspended PM) as well as water (chemicals, leakages, discharges), and would also lead to a rise in GHGs (CO_2, CO, NO_X, SO_X, O_3, CH_4) that further instigates increment in LST (Ministry of Statistic and Programme Implementation, 2015). Quantification of LST largely depends upon atmospheric parameters including atmospheric transmittance, upwelling and downwelling radiance, atmospheric water vapor content; sensor parameters such as viewing angle, sensor calibration, spectral range; surface parameters (surface albedo, land surface emissivity); and condition of the atmosphere (cloud cover) when the data are captured. Some of the selected (latest) studies performed by various researchers that relate LST and LULC (for reference) are as shown in Table 14.1.

A rise in LST not only critically affects the health and welfare of urban dwellers but also of the ones residing in rural as well as suburban areas. Elevated LST can affect us in multiple ways such as causing power outages, deteriorating the quality of air and water, causing severe health issues, affecting the thermal comfort, leading to food and water crisis, rising intensity and frequency of extreme weather events, and increasing mortality rates. Rise in LST also gives rise to a phenomenon of UHI that is an issue of serious concern these days.

3. Urban Heat Island

As a result of increased demographic pressure and in turn alteration in landscape toward increasing urban areas, cities these days are more susceptible to heatwaves and UHI phenomenon. This has now extended to such levels that the UHI effect is becoming a common phenomenon, is getting stronger, and is continuing for longer durations, which further aggravates thermal risk for the inhabitants (Founda and Santamouris, 2017). UHI is a phenomenon observed in cities, where the city's temperature becomes higher compared to the nearby suburban or rural areas (Liang and Shi, 2009).

Table 14.1 Literature—relationship between land surface temperature and urban landscape.

Author	Inference
Qian et al. (2020)	Retrieved LST and emissivity from ground-based time-series thermal infrared data
Nimish et al. (2020)	Explored temperature indices by deriving a relationship between LST and urban landscape
Guha et al. (2020)	Performed long-term analysis on relationship between LST and built-up index (NDBI)
Wang and Murayama (2020)	Performed geosimulation of LULC scenarios and identified their impacts on LST for Sapporo, Japan
Mustafa et al. (2020)	Compared four algorithms to predict LST using Landsat data
Daramola et al. (2018)	Assessed thermal response of variations in the landscape of an urban area
Chandra et al. (2018)	Performed geospatial analysis on the city of Jaipur, India, to demonstrate a linkage between urban expansion and LST
Tran et al. (2017)	Characterized relationship between changes in LULC and LST
Pal and Ziaul (2017)	Detected LULC changes and LST for pre-monsoon, monsoon, and post-monsoon over English Bazar urban center
Youneszadeh et al. (2015)	Studied the effect of LU changes on LST over the Netherlands
Yu et al. (2014)	Compared various LST retrieval methods/algorithms
Bharath et al. (2013)	Studied LST responses to landscape dynamics over central Western Ghats in India
Sobrino et al. (2006)	Derived LST using an airborne hyperspectral thermal infrared scanner

These can be inferred to the difference in the percentage of vegetation, water, and impervious surface. UHIs can be divided into two categories:

1. Atmospheric UHI (AUHI): As a result of absorption of heat in the air due to the presence of particles, air temperature increases causing AUHI effect. It is further classified into two categories based on height: canopy layer UHI (heat islands present in air layer from surface level to the top of buildings or vegetation), and boundary layer UHI (heat islands present in the region above rooftops and vegetation).
2. Surface UHI (SUHI): This occurs as a result of higher surface temperatures in urban areas due to the presence of large region covered with impervious surfaces.

Some of the causal factors of UHI are multiple internal reflections, higher absorption of shortwave radiations, rise in anthropogenic heat sources, hindrance in the transmission of longwave radiations, lower evapotranspiration rates, changes in wind gust and turbulence, reduction in radiative cooling, etc. (Dash et al., 2002). The main reasons behind these factors are the difference in the thermal properties of materials used for construction in urban areas when compared to the naturally occurring and imbalance in the composition of the landscape over a region. As a result of the difference in heat storage capacity of materials, the latent and sensible heat budget varies, leading to changes in the convective and advective energy flow (Oke, 1982; Roth, 2012). Fig. 14.1 shows a schematic representation of surface temperatures in urban, suburban, and rural areas.

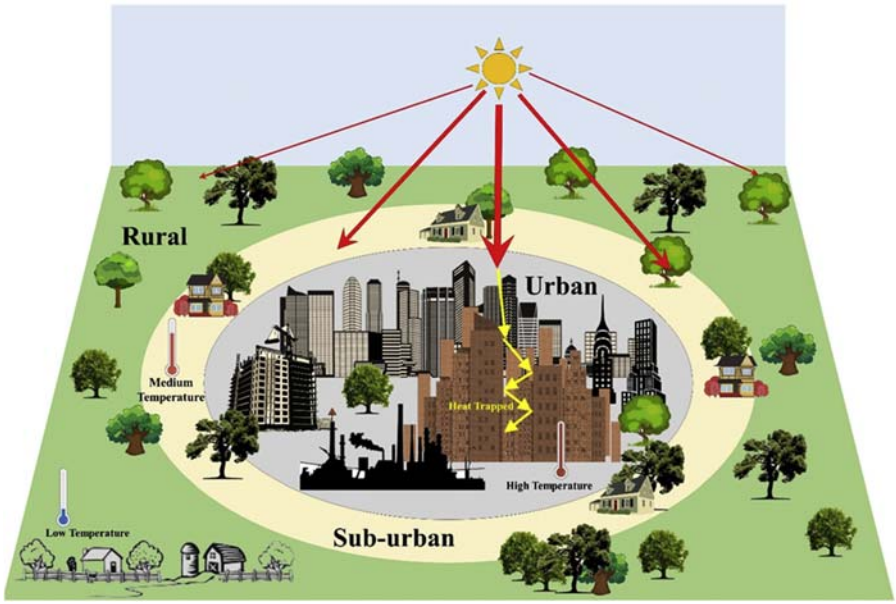

FIGURE 14.1

Temperature distribution in urban, suburban, and rural areas signifying UHI.

Understanding UHI phenomena is one of the biggest challenges for the scientific community as it is directly related to providing apt infrastructure and a suitable environment for the residents (Stewart, 2011). Interpretation of UHI was first studied in 1833 by Luke Howard over London, where he noticed the city center being warmer when compared to the countryside (Mills, 2008). His annotation was then noticed and motivated many researchers raising concern regarding the exclusion of meteorology in the field of science. This triggered a need to perform UHI and LST studies over the cities as shown in Table 14.2.

The continual rise in surface temperature leads to discomfort that further increases energy consumption due to the increased usage of various electronic devices such as air conditioning and water coolers. This leads to increment in concentration of GHGs in the atmosphere leading to rising air temperatures that further instigates UHI. Rise in UHI is one of the most critical parameters to increase surface temperature. Thus this vicious cycle continues, further damaging human health and welfare. UHI not only affects human health but also disrupts complete urban ecological system. It affects the microclimate of the region and exerts tremendous pressure on the floral and faunal diversity especially on the ones that are sensitive to alteration in temperature. UHI also affects the evapotranspiration rates, that alters the moisture content in the atmosphere and earth's surface. Increased frequency and intensity of UHI can have numerous impacts on human health and welfare that includes cramps due to heat, difficulty in breathing and other pulmonary diseases, thermal discomfort, lethal and nonlethal heat strokes, exhaustion, etc. (EPA, 2019). UHI is one of the key factors that lead to the generation of heatwaves and is solely responsible for many deaths.

Table 14.2 Literature—LST and UHI studies over cities.

Author	Inference
Sarif et al. (2020)	Assessed alterations in LULC and LST, further identified their impact on SUHI over Kathmandu Valley for a period of 30 years
Oh et al. (2020)	Used deep learning algorithm for forecasting the magnitude of UHI in Seoul and introduced a new index for determining the same
Kimuku and Ngigi (2017)	Studied urban heat island trends and simulated LST for 2025 across Nakuru county in Kenya for aiding in urban planning
Mathew et al. (2016)	Estimated UHI over the city of Chandigarh over a period of 4 years
Grover and Singh (2015)	Performed UHI analysis on Mumbai and identified the major sectors behind the rise of UHI
More et al. (2015)	Compared estimation of UHI using LST and ambient air temperature
Murata et al. (2013)	Calculated UHI by simulating biases in surface air temperature using regional climatic model for Japan
Wolters and Brandsma (2012)	Estimated UHI in residential areas of Netherlands using weather amateurs
Gedzlman et al. (2003)	Performed UHI analysis over New York City and identified the intensity throughout the day
Yamashita (1996)	Estimated and compared UHI intensity over seasonal basis for Tokyo

4. Significance of studying LST and UHI

As per a review paper published in *Environmental Research Letters*, 97% of the studies established that human-induced changes are the key source of rising global warming and climate change (NASA, 2018). As per Jordon (2007), there are sufficient studies to prove and infer that the surface temperature of the earth is changing significantly at an alarming pace and is an issue of serious concern. As per a report by UN DESA (2018), 54% of the global population already reside in urban areas which are predicted to increase at a faster rate in the near future, majorly being concentrated in developing countries (Chen et al., 2014). Exceptional rise is LST, and the phenomenon of UHI, affects almost all the sectors on which our life depends. These sectors include

- Energy: Higher energy consumption due to increased usage of air conditioning, irrigation, and rise in fuel requirement in the transportation sector (Scott et al., 1990).
- Agriculture: Crop failure can affect food security.
- Water resources: Changes in the natural water cycle as a result of alteration in the rate of evaporation and precipitation. Melting of ice caps can also result in the rise of sea level causing huge concern for the coastal cites (Bolin et al., 1986).
- Forest: Rising temperatures can exert stress on few species, thus making them vulnerable for fire, disease, and pest infection.
- Ecosystem biodiversity: Not every flora and fauna can sustain large-scale changes in temperatures, thus, can gradually become endangered or even extinct (Davis, 1989).
- Air quality: Air pollution levels and temperature are interdependent and rise in one can lead to an increment in the other.

- Infrastructure: Rising LST can affect the construction material of the available infrastructure and can lead to bending or breaking of some critical joints. Damage can be in the form of material as well as life.
- Marine life: Alteration in temperature affects marine biodiversity as a result of migration of few species from one area to other (as they are unable to acclimatize to higher temperatures) or can even lead to mass extinction (Science for Environmental Policy, 2007).
- Human health: The increasing temperature can lead to increased skin diseases, asthma, migraine, stress, hay fever, and vector-borne diseases (Raloff, 1989).

5. Theoretical background

Electromagnetic spectrum can be divided into various segments based on wavelength range, and their intensity varies with the transmission allowed by the atmospheric windows. One of the regions is dedicated to thermal remote sensing that can be defined between the wavelength range of 3−35 μm. Within this range, an excellent atmospheric window lies between 10 and 12 μm and thus, this region is used for various applications. The surface energy budget is a combination of radiative and nonradiative elements (Santra, 2019). Radiative elements include incoming shortwave and outgoing longwave radiations, while latent heat and sensible heat form nonradiative components. Net energy is the summation of downward (heating of earth's surface) and upward (summation of reradiated energy and reflected radiation of the earth's surface) radiation. Two of the primary parameters that influence thermal remote sensing are albedo and land surface emissivity. Albedo can be defined as the fraction of the total energy incident on a surface that gets reflected (Oke and Cleugh, 1987). Albedo varies with surface properties (type, shape, color, and size of the surface), angle of incidence, amount of aerosols and water vapor content in the atmosphere, and distribution of solar energy. Land surface emissivity can be elaborated as the ratio of energy radiated by any material to the energy emitted by a blackbody at the same wavelength and viewing angle under similar atmospheric conditions. This depends upon the composition of the material, surface roughness, and viewing angle (Li et al., 2013). Application of thermal remote sensing can be explained via three basic laws as mentioned below:

- **Stephan−Boltzmann law:** explains the relationship between energy radiated and the temperature of an object as shown in Eq. (14.1). The law signifies that any object above 0K emits energy equivalent to the fourth power of its absolute temperature.

$$E = \sigma T^4 \tag{14.1}$$

Here, E = Energy emitted; σ = Stephan−Boltzmann constant; T = Temperature in Kelvin.

- **Wein's displacement law:** states that radiation by blackbody will reach its peak at different temperatures depending on its wavelength. Higher the temperature, it will have peak radiation at lower wavelengths. Mathematically it can be expressed as Eq. (14.2).

$$\lambda_m \times T = 2897\ \mu mK \tag{14.2}$$

Here, T = Temperature in Kelvin; λ_m = Wavelength at which maximum radiation is achieved.

This law also explains how thermal range for the earth's surface is obtained. Considering average temperature of earth's surface as 300K (27°C), then as per Eq. (14.2), the wavelength at which peak radiation is obtained comes out to be 9.66 μm.

- **Planck's law/function:** relates spectral radiance of a blackbody or nonblackbody with its temperature and is the basis of deriving LST using thermal remote sensing. Since there is no blackbody, emissivity is used with blackbody radiance to derive nonblackbody radiance (Eq. 14.3) and further temperature.

$$R_{\lambda,\,T} = \varepsilon_\lambda \times B_{\lambda,T} = \varepsilon_\lambda \times \frac{C_1 \times \lambda^{-5}}{\pi\left[e^{\frac{C_2}{\lambda T}} - 1\right]} \tag{14.3}$$

Here, $R_{\lambda,T}$ = Spectral radiance of nonblack body at wavelength λ and temperature T (in $Wm^{-2}\mu m^{-1}sr^{-1}$); $B_{\lambda,T}$ = Spectral radiance of black body at wavelength λ and temperature T (in $Wm^{-2}\mu m^{-1}sr^{-1}$) [Planck's radiation law]; λ = Wavelength (μm); T = Temperature (K); ε_λ = emissivity of the body at wavelength λ; C_1 and C_2 are radiation constants.

The surface temperature of objects with a Lambertian surface with known emissivity can be determined as shown in Eq. (14.4).

$$T = \frac{C_2}{\lambda \ln\left(\frac{\varepsilon_\lambda C_1}{\pi\lambda^5 R_{\lambda,T}} + 1\right)} \tag{14.4}$$

6. Practical example

This section of the chapter provides a case study to understand the effect of increasing urbanization on the land surface temperature. Further, it deals with the estimation of UHI index and concluded with the suggestion of mitigation measures for minimizing the discomfort of the residents. The following subsection provides detailed information about the study area, method used, and observed results.

6.1 Introduction and study area

Kolkata Metropolitan Area (KMA), also termed as Greater Kolkata, was chosen for the analysis as shown in Fig. 14.2. A buffer of 10 km was also considered around the boundary to understand UHI's phenomenon over the metropolitan. The city of Kolkata holds a significant position in Indian history as it was the first capital of British India and is one of the oldest metropolitan cities in India. It serves as a capital city for the Indian state of West Bengal and is located on the bank of river Hooghly. The metropolitan shares its boundary with the Indian state of Assam and Sikkim, along with an international boundary with Bangladesh. The metropolitan serves as a domineering center for Indian art, literature and is home to several architecture heritages. Earlier most of the metropolitan region was a wetland but as a result of increased movement of people and rising urbanization, it was converted into urban settlements. Later in August 2002, the undeveloped and the remaining part of wetlands were designated as Ramsar site, thus providing it with an environmental value.

The metropolitan is spread across an area of 1886.67 km^2 and has an elevation of 1.5−9 m above MSL (mean sea level). As per Köppen climate classification, it has a tropical wet and dry climate. The mean annual temperature and rainfall over the city estimate to 26.8°C and 1850 mm, respectively.

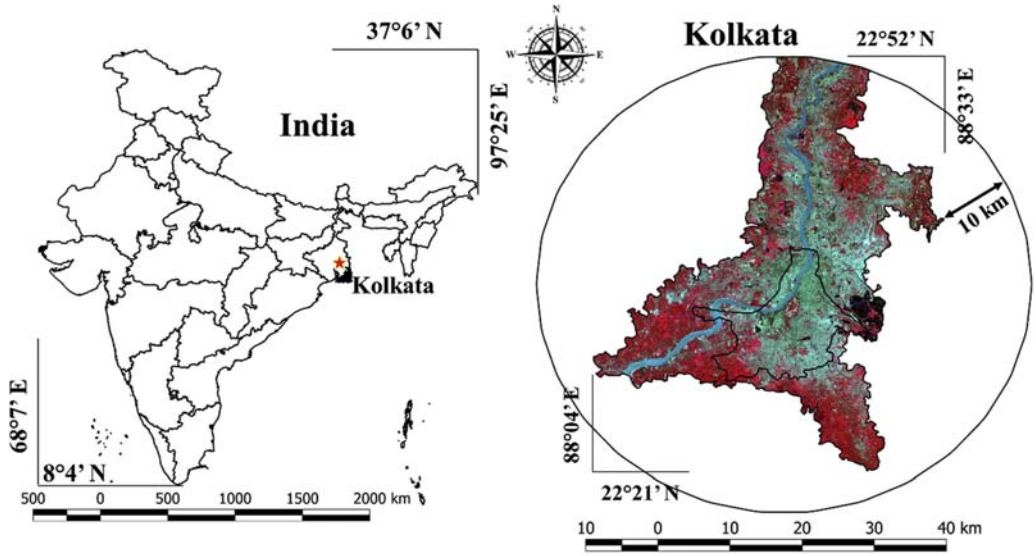

FIGURE 14.2

Study area depicting KMA and its location in India.

The region experiences four seasons—summer (March to June), monsoon (June to September), post-monsoon autumn transition (September to November), and winter (December to February). The minimum winter temperatures range from 9 to 11°C, while the maximum summer temperature often exceeds >40°C. The population curve of the metropolitan is as shown in Fig. 14.3.

The metropolitan is home for several esteemed historical, cultural, and academic institutions of great national importance. It has many public and private sector industrial units including steel, minerals, heavy engineering, mining, electronics, textile, tobacco, food processing, and jute.

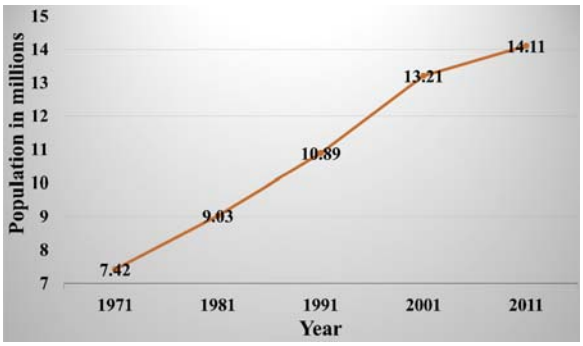

FIGURE 14.3

Demographic information of Kolkata Metropolitan Area.

The region also houses the headquarters of various companies such as ITC Limited, Coal India Limited, Exide Industries, Britannia, etc. The city is connected via a good transportation system (road, rail, and air) with other parts of India as well as internationally. All this has contributed to the large-scale migration that has led to the development of the city with enormous landscape changes. The infrastructure of the region is highly diverse where few parts of the city have congested growth, old architecture, overpopulated slums, heavily crowded markets places, ramshackle buildings and narrow alleyway. In contrast, the other has a completely planned architecture with ample open and vegetated space. As a result of enormous growth and changes in urban pattern and structure of the metropolitan, numerous problems are being faced by the residents including a rise in pollution levels, increased level of discomfort, heat stress, and rise in the level of RSPM (respirable suspended particulate matter) that has led to increased cases of people with pulmonary related diseases. The city is facing various environmental problems that have affected the microclimate of the region in terms of surface temperature that has further led to increased intensity and days of UHI.

6.1.1 Method used

A five-step process as shown in Fig. 14.4 was involved in the research work to fulfill the main objective. It includes: (1) Data acquisition and preprocessing, (2) Land use analysis, (3) Quantification of emissivity and Land Surface Temperature, 4) Estimation of Normalized Urban Heat Island Index (NUHII), (5) Derivation of relationship between LU and LST

- Data acquisition and preprocessing: Primary and secondary data used for the analysis include Landsat series (5 = thematic mapper and 8 = operational land imager/thermal infrared), city development plan, survey of India toposheets (1:50,000 scale), ground truth/collected data, data obtained from Google Earth pro and Bhuvan. CDP was georegistered using GCPs (ground control points) obtained from Google Earth and ground collected data. Toposheets, CDP, and maps from Bhuvan were used to delineate the boundary of Kolkata Metropolitan Area (KMA). All the remote sensing data were then corrected for any geometric errors and was resampled with the help of ancillary data. All the required bands were then cropped pertaining to the study area.
- Land use analysis: Land use analysis was performed using a supervised classification technique and was estimated using four steps. At first, False Color Composite (FCC) was generated, which involves assigning blue color to green band, green color to red band, and red color to near-infrared (NIR) band. FCC is useful as it can help in easy identification of certain features due to the presence of heterogeneity among various classes in urban areas. In the second step, representative training polygons for each class were digitized taking into account the heterogeneity and interclass variations using FCC. These polygons were then converted into signature by using mean and covariance matrix (obtained from overlapping polygons and FCC). In the third step, classification was performed using Gaussian maximum likelihood classifier that takes into account the probability density function for assigning the class to each pixel. Four classes, namely, urban, vegetation, water, and others, were considered for this analysis. Mathematically the algorithm can be defined as shown in Eq. (14.5).

$$X \varepsilon Cj, \text{ if } p(Cj/X) = \max[p(C1/X),\ p(C2/X), \ldots, p(Cm/X)] \tag{14.5}$$

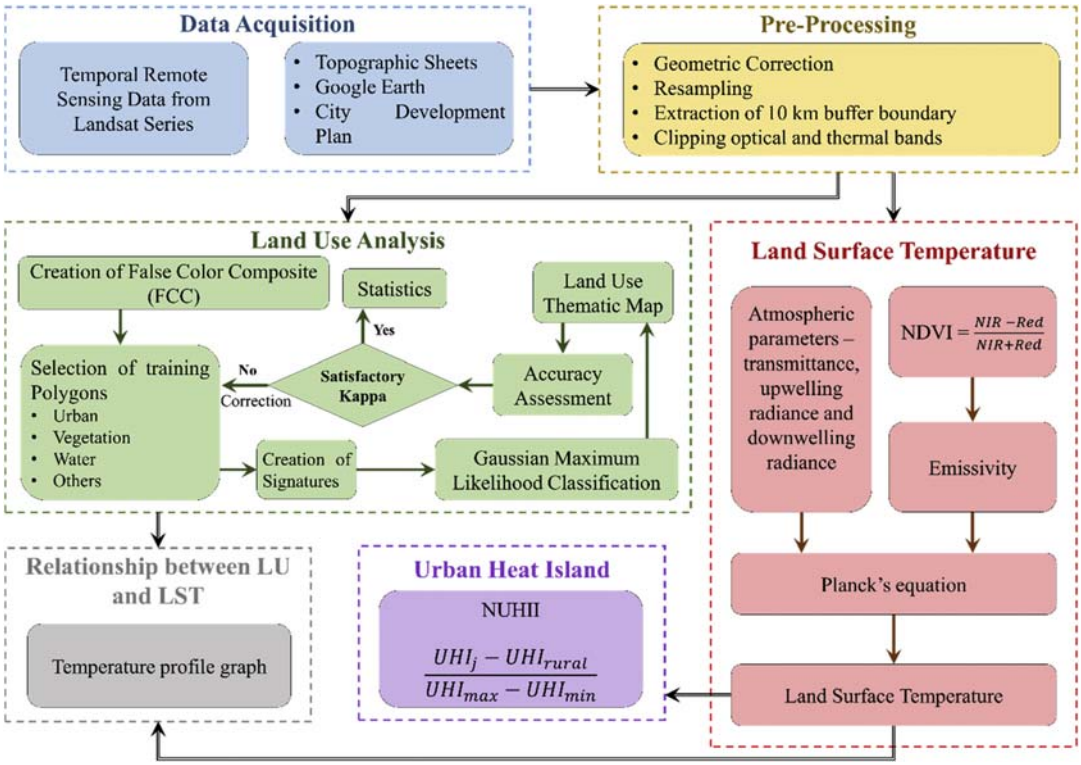

FIGURE 14.4

Method.

Here, p(Cj/X) denotes the conditional probability of pixel X being a member of the class; max [p(C1/X), p(C2/X), …, p(Cm/X)] is a function that returns the largest probability among four categories.

The last step of land use analysis was accuracy assessment which was performed by comparing the classified map obtained from GMLC algorithm and validation map obtained from Google Earth and ground truth data for 2019. For historical years, the classified map was created using 70% of the signatures and validation map was created from the remaining ones. These maps, when compared to each other, generated a confusion matrix that was further used to estimate overall accuracy and kappa coefficient (measures of accuracy).

- Quantification of emissivity and LST: Emissivity was estimated using NDVI threshold method. This method considers mixed pixels of soil and vegetation and assigns values to them based on the proportion of vegetation. A thorough literature review was conducted to obtain the emissivity values of pure water, soil, and vegetation class ($\varepsilon_{water} = 0.9910$, $\varepsilon_S = 0.9668$, $\varepsilon_V = 0.9863$). The formulas used for estimation of emissivity are as shown in Eqs. (14.6)-(14.8).

$$\varepsilon_{SV} = \varepsilon_V P_V + \varepsilon_S(1 - P_V) + C \tag{14.6}$$

Here,

ε_{SV} → emissivity of soil + vegetation
ε_V → emissivity of vegetation
ε_S → emissivity of soil

$$P_V = \left(\frac{NDVI_i - NDVI_S}{NDVI_V - NDVI_S}\right)^2 \tag{14.7}$$

Here,

P_V → proportion of vegetation
$NDVI_i$ → Normalized Difference Vegetation Index of the pixel under consideration
$NDVI_S$ → NDVI of pure soil
$NDVI_V$ → NDVI of pure vegetation

$$C = (1 - \varepsilon_S)\varepsilon_V F(1 - P_V) \tag{14.8}$$

Here,

C → constant defining surface characteristics
F → geometrical factor (depends on surface geometry, usually considered 0.55)

Postestimation of emissivity, LST was quantified using Radiative Transfer Equation (RTE) that takes surface (emissivity) and atmospheric parameters (atmospheric transmittance, upwelling radiance, and downwelling radiance) into account. A simplified RTE can be expressed as shown in Eq. (14.9).

$$B_i(T_i) = \tau_i\left[\varepsilon_i B_i(T_s) + (1 - \varepsilon_i)I_i^{\downarrow}\right] + I_i^{\uparrow} \tag{14.9}$$

Here,

$B_i(T_i)$ → top-of-atmosphere radiance received at the sensor for channel i having T_i at-satellite brightness temperature; it can be obtained by using gain and offset value
τ_i → atmospheric transmittance for channel i
ε_i → emissivity for channel i
$I_i^{\downarrow}$ → downwelling radiance
$I_i^{\uparrow}$ → upwelling radiance

Planck's equation can be further expressed as shown in Eq. (14.10).

$$B_i(T_s) = \frac{2hc^2}{\lambda_i^5 \times \left(e^{\frac{hc}{\lambda_i kT_s}} - 1\right)} \tag{14.10}$$

Here,

h → Planck's constant = 6.626×10^{-34} J s
c → speed of light = 2.98×10^8 m/s
λ_i → effective wavelength for channel i
k → Boltzmann constant = 1.3806×10^{-23} J/K
T_s → Land Surface Temperature

Eqs. (14.9) and (14.10) were then rearranged to get Eq. (14.11) which was utilized for estimating LST:

$$T_s = \frac{C_1}{\lambda_i \times \ln\left(\frac{C_2}{\lambda_i^5\left(\frac{B_i(T_i) - I_i^{\uparrow} - \tau_i(1-\varepsilon_i)I_i^{\downarrow}}{\tau_i \varepsilon_i}\right)}\right)} \tag{14.11}$$

Here,

$C_1 \rightarrow 14{,}387.7\ \mu m\ K.$

$C_2 \rightarrow 1.19104 \times 10^8\ W\ \mu m^4\ m^{-2}\ sr^{-1}$

Atmospheric parameters including transmittance, upwelling, and downwelling radiance were estimated by using an online calculator as provided by NASA (https://atmcorr.gsfc.nasa.gov/). The calculator considers geographic coordinates; information about the type of sensor; year, month, date, and time of image captured and surface meteorological parameters (temperature, the altitude of mounted sensor, pressure, and relative humidity). These parameters along with emissivity values were provided in Eq. (14.11) to obtain LST. Further, interclass variability was assessed using the Coefficient of Variation (CoV) as shown in Eq. (14.12). CoV is a statistical parameter that defines how distributed the surface temperature is within the same land use class.

$$CoV = \frac{\sigma}{\mu} \times 100 \tag{14.12}$$

Here, CoV = Coefficient of Variation (%), σ = Standard deviation, μ = mean.

- Estimation of Normalized Urban Heat Island Index (NUHII): NUHII is an index that can define the intensity of heat islands across the area of interest. This index was evaluated by estimating LST for only urban area (extracted using land use classification map and LST map obtained in previous subsections) for 2019. LST for few areas with low-density urban and very small urban pockets in the study area's buffer region was averaged out to get the LST of rural area. NUHII was then estimated using 13.

$$NUHII = \frac{(LST_i - LST_{Rural})}{(LST_{max} - LST_{min})} \tag{14.13}$$

- Derivation of relationship between LU and LST: This was performed by overlaying land use maps and LST maps on each other. A transact "A-B" was then considered over LU map such that it covered all the classes. LST values corresponding to this transact were considered to create a temperature profile graph. This graph represented the LST values for each LU class over the transact, and variations were estimated.

6.1.2 Results and discussion

- Land use analysis: Temporal analysis was performed over the KMA region with 10 km buffer for 2000, 2004, 2009, 2014, and 2019. Figs. 14.5 and 14.6 depict the land use map and percentage coverage of each land use class over the study region. A three-fold rise in urban class was observed across the study area with an infill type of development in the core of the metropolitan and development or swelling of urban pockets in the buffer especially in the North direction. It was observed that the alterations were at the cost of vegetation and others category. Over the years, vegetation and others category have reduced drastically by 18% and 13.82%. However, the water classes have increased slightly due to the complete utilization of available landscape that is dedicated to the Eastern wetlands (Ramsar site).
- Land Surface Temperature: Land Surface Temperature for the metropolitan with 10 km buffer was quantified, as shown in Fig. 14.7. It was observed that the mean LST of the region has increased from 19.15 to 29.74°C. The minimum and maximum surface temperature of the study area has also experienced a significant rise. Post this, a classwise analysis was performed wherein each land use class was extracted, and LST corresponding to them was calculated. Fig. 14.8 illustrates the minimum, maximum, and mean values of surface temperature and estimated CoV for understanding variation due to each land use class and within each of the class. It was observed that the highest surface temperature corresponds to urban class, followed by others and vegetation category. Water class including ponds, lakes, wetlands, aquaculture, and river

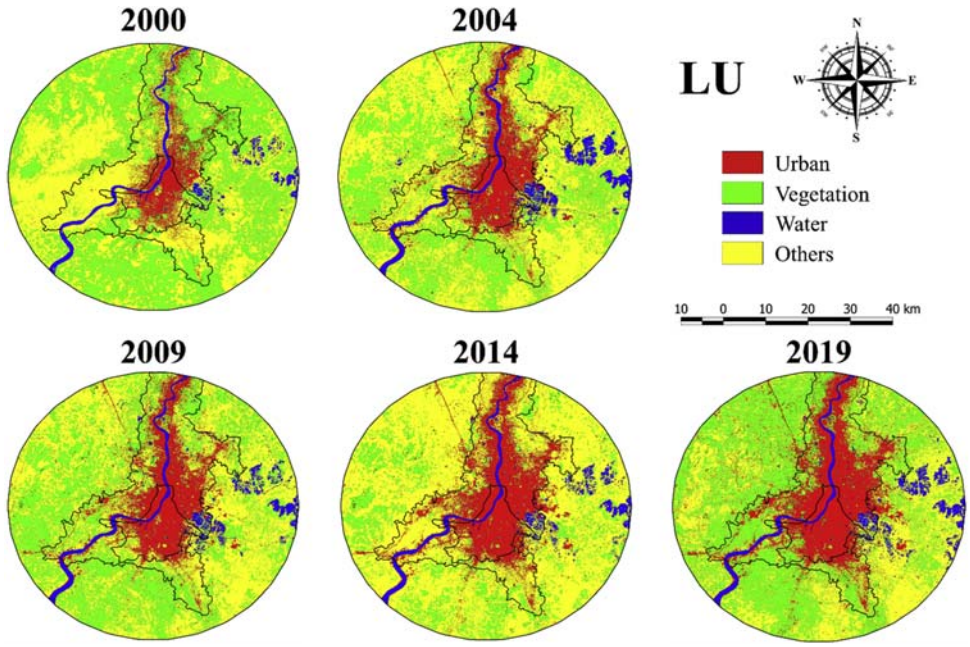

FIGURE 14.5

Land use maps for KMA with 10 km buffer.

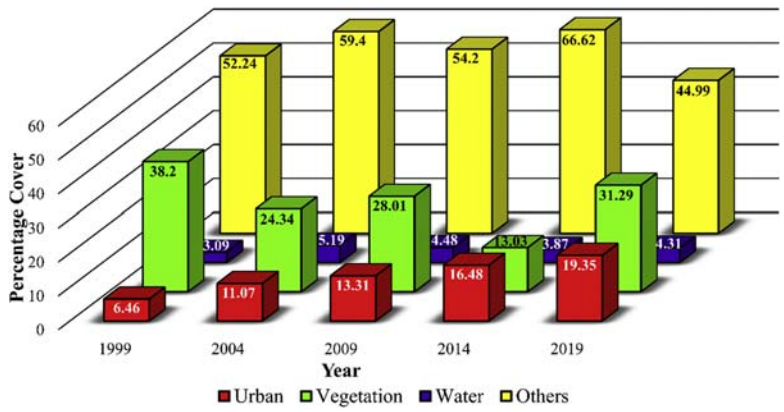

FIGURE 14.6

Classwise statistical analysis of LST from the study area.

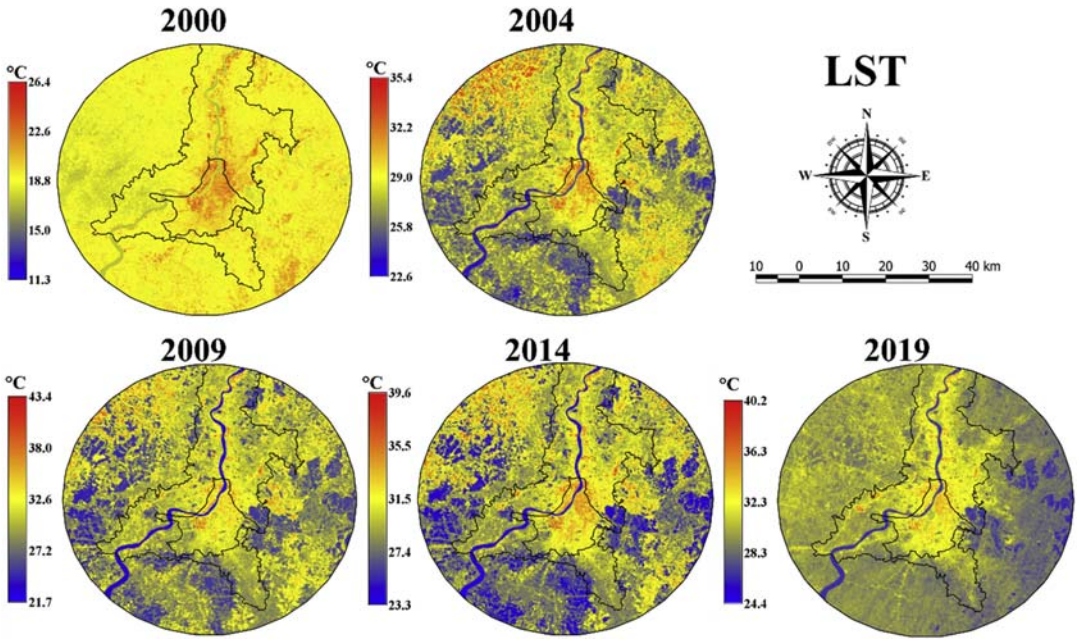

FIGURE 14.7

Temporal land surface temperature maps for KMA with 10 km Buffer.

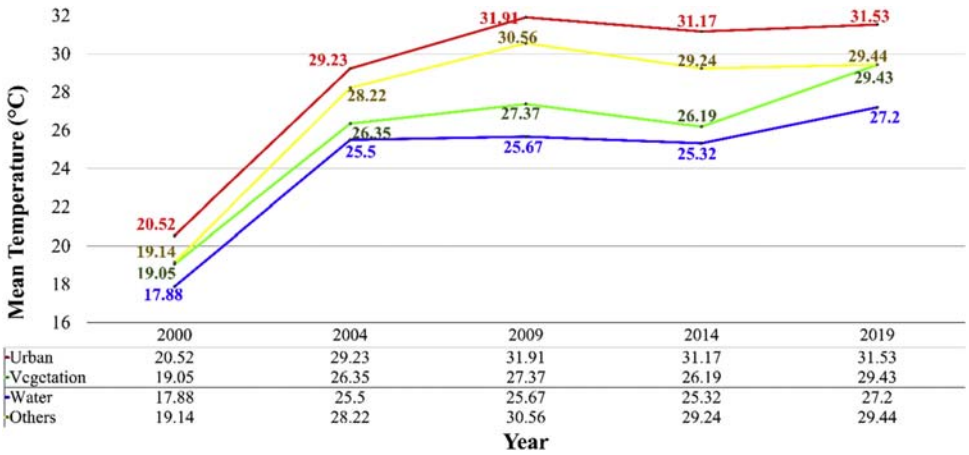

FIGURE 14.8

Classwise statistical analysis of LST from the study area.

corresponded to minimum surface temperature. It was visible from the results that each land use class has experienced a rise in minimum, maximum, and mean surface temperature. Rise in LST for urban class can be explained with the changes in the land use where there has been a significant rise observed in urban area, and these areas have high heat storage capacity. Rise in LST of vegetation and other class can be explained by the reduction in density of vegetation and breathing spaces. The rise in LST of water bodies can be inferred to the increased area of wetlands because these have higher surface temperature than other deeper water bodies.

- Normalized Urban Heat Island Index (NUHII): NUHII obtained was then reclassified into six classes wherein first class represented negative heat islands and rest of them with the increasing class value corresponded to increased positive UHI. The reclassified NUHII for the study area is shown in Fig. 14.9 and it was found that most of the anthropogenic constructions exhibit positive UHIs. The highest values were observed in the core region and few urban pockets toward the western part due to increased developments. More than half of the urban area has NUHII value of 0.1−0.3 that affects more than 70% of the residents. One-tenth of the study region was observed to experience very high positive heat islands. Approximately 80% of the core part of metropolitan was observed to have a positive UHI that can be inferred to the domination of urban surface over any other class. Percentage area cover under each class is as shown in Table 14.3.
- Derivation of relationship between LU and LST: The LU and LST maps obtained in the study for 2019 were examined to comprehend surface temperatures corresponding to each LU class. A transact A-B was considered across LU map, and temperature profile graph was created as illustrated in Fig. 14.10. It was observed that high value or the crest signifies the presence of urban or others category while moderate/low values or dips correspond to the presence of vegetation and water bodies, respectively. It can be inferred that presence of vegetation and water bodies in the region can help in regulating the microclimate of the region, while construction of impervious surfaces or leaving surface bare can lead to a rise in the surface temperatures.

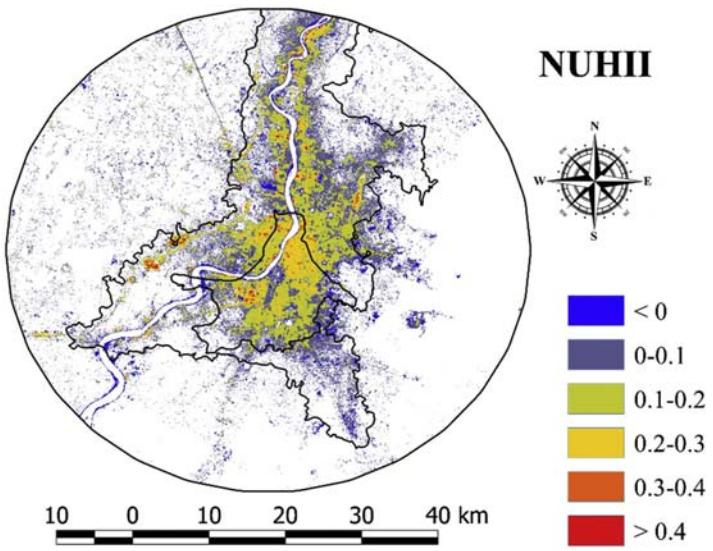

FIGURE 14.9

NUHII for KMA region with 10 km buffer for 2019.

Table 14.3 UHI type and percentage cover.

Category	Range	UHI type	Percentage coverage
1	<0	Negative	19.18
2	0−0.1	Weak	39.45
3	0.1−0.2	Low	30.78
4	0.2−0.3	Moderate	8.55
5	0.3−0.4	High	1.64
6	>0.4	Extreme	0.40

7. Mitigation measures

There are several criteria at the building level, neighborhood level, community level, building design level, and meso-town level that can help in reducing the overall UHI effect by reducing the surface temperatures. Few of them includes understanding the ratio of building height to width of the street, the orientation of the building, reflectivity of the surface, conductivity of materials, and the presence of urban cooling spaces. Some necessary mitigation measures that can be considered for reducing the overall LST and UHI in the city are as follows:

- Shading: Providing provision of shading on building entries, streets, and public ventures with the help of artificial structures or greenery.

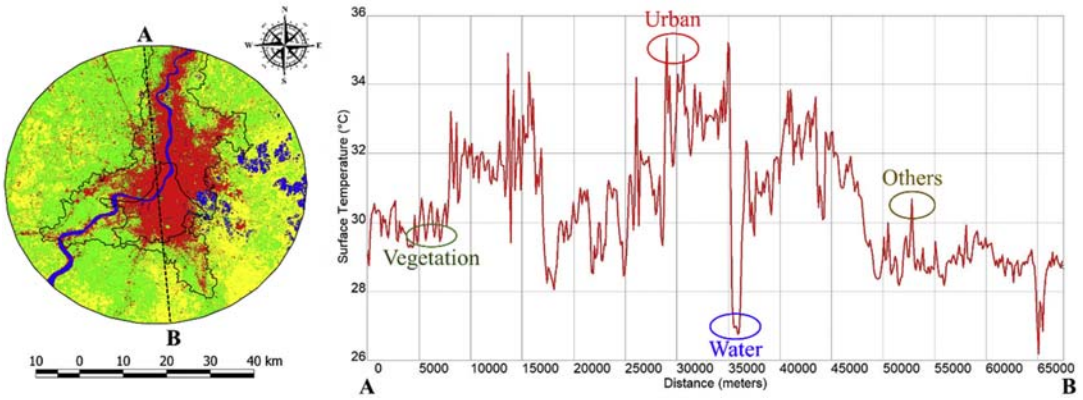

FIGURE 14.10

Temperature profile graph for KMA considering 10 km buffer.

- Mini forest: Dedicating a small area for vegetation and planting native species of trees in every locality.
- Development of gardens: Considering that the free space available is small, then it can be converted into parks or community gardens.
- Water-sensitive urban design: Developing ponds, pools, and fountains in every locality or installation of hybrid systems such as wind towers and sprinklers. Another advantage associated with this measure is that it improves the aesthetics and beauty of the locality.
- Building design and planning: Introduction of cool roofs and green roof can reduce the overall heat storage. Avoiding dark color paints and using high reflectivity materials for building exteriors can be implemented as a part of the design. Another design intervention can be construction of vertical gardens on the external surface of building walls.
- Road infrastructure: Constructing road with cooler material instead of asphalt or painting roads with white color can increase the reflectivity and reduce the overall heat storage capacity.
- Creation of pollution-free zones: Few areas and the city's main markets can have no vehicle policy, i.e., a complete ban on vehicles throughout the day or for a few hours.
- Green power generation: Government can introduce some incentives for green power generation at the individual level or can even set up a few power generation plants that use a cleaner source of energy.
- Behavior change: Outreach program and other strategies can be created to make people environmentally educated. These programs can be associated with
  - ➢ Reduction in the usage of private cars along with promoting carpooling and public transport
  - ➢ Teaching residents to avoid misuse of electricity/power and other available resources
  - ➢ Installation of a cleaner source of energy at individual, community, or city level

8. Conclusion

This chapter provided insight into how unplanned and rapid urbanization can affect a region's surface temperature. The study sets out to understand how LST leads to the development of UHI and further affects the residents' health and welfare. The research also provided a practical example of how the study of UHI can be performed supplemented with an estimation of LST and development of LU. The key purpose of this study was to provide the effects of UHI and suggest mitigation measures for reducing them. One of the most important take away points from this chapter is that a rise in impervious surfaces can significantly alter the microclimate of a region in terms of LST that further instigates or increases the intensity and frequency of positive UHIs. Altogether, unplanned and unregulated urbanization with lesser vegetation, open spaces, and water bodies can lead to a rise in warming throughout the urban area and increases heat-related issues among the residents. Therefore, it can be concluded that plantation of dense vegetation rather than fragmented ones and the presence of water bodies throughout the urban area can solve the problem of high surface temperature and ill-effects of UHIs. Open spaces in the city serve as regions where high pollutants and other dust particles can be displaced properly and avoid them being blocked within the localities in a city, thus creating breathing spaces. The study was complemented by practical example performed for KMA with 10 km buffer, and it was observed that the study area has experienced tremendous growth in terms of impervious surface on the cost of vegetation and others category that has led to an average rise of 10.6°C in surface temperature.

Further, the relationship between LU and LST was derived, and it was inferred that urban areas and barren grounds contribute to high, vegetation corresponds to moderate, and water bodies corresponds to low surface temperatures. The final part of this chapter deals with the suggestion of a few mitigation measures to tackle the rising issue of UHI. The information provided in this chapter and other research findings can act as background data and suggestions to the urban planners, stakeholders, and decision-makers to reformulate the older and develop new policies for achieving sustenance.

References

AATSR and SLSTR, 2018. LST Portal: Welcome to the AATSR/SLSTR Land Surface Temperature Portal. Retrieved from: http://lst.nilu.no/ (Accessed 10 March 2018).

Aggarwal, S.P., Garg, V., Gupta, P.K., Nikam, B.R., Thakur, P.K., 2012. Climate and Lulc change scenarios to study its impact on hydrological regime. In: ISPRS - International Archives of the Photogrammetry, Remote Sensing and Spatial Information Sciences, vol. 34, pp. 147–152.

Anderson, M.C., Norman, J.M., Kustas, W.P., Houborg, R., Starks, P.J., Agam, N., 2008. A thermal-based remote sensing technique for routine mapping of land-surface carbon, water and energy fluxes from field to regional scales. Remote Sens. Environ. 112, 4227–4241.

Bento, V.A., DaCamara, C.C., Trigo, I.F., Martins, J.P.A., Duguay-Tetzlaff, A., 2017. Improving land surface temperature retrievals over mountainous regions. Remote Sens. 9 (1), 38–50.

Bharath, S., Rajan, K.S., Ramachandra, T.V., 2013. Land surface temperature responses to land use land cover dynamics. Geoinfor. Geostat. 1 (4), 1–10.

Bolin, B., Doos, B.R., Jaeger, J., Warrick, R.A. (Eds.), 1986. The Greenhouse Effect, Climatic Change, and Ecosystems, Scope 29. Wiley, Chichester, West Sussex.

Chandra, S., Sharma, D., Dubey, S.K., 2018. Linkage of urban expansion and land surface temperature using geospatial techniques for Jaipur City, India. Arabian J. Geosci. 11 (2), 1–12.

Chen, M., Zhang, H., Liu, W., Zhang, W., 2014. The global pattern of urbanization and economic growth: evidence from the last three decades. PLoS One 9 (8), 1–15.

Daramola, M.T., Eresanya, E.O., Ishola, K.A., 2018. Assessment of the thermal response of variations in land surface around an urban area. Model. Earth Syst. Environ. 4 (2), 535–553.

Dash, P., Göttsche, F.M., Olesen, F.S., Fischer, H., 2002. Land surface temperature and emissivity estimation from passive sensor data: theory and practice-current trends. Int. J. Remote Sens. 23 (13), 2563–2594.

Davis, M.B., 1989. Address of the past president: Toronto, Canada, August 1989: insights from paleoecology on global change. Bull. Ecol. Soc. Am. 70 (4), 222–228.

EPA, 2019. Heat Island Impacts. Retrieved from: https://www.epa.gov/heat-islands/heat-island-impacts (Accessed 11 January 2021).

Founda, D., Santamouris, M., 2017. Synergies between urban heat island and heat waves in Athens (Greece), during an extremely hot summer (2012). Sci. Rep. 7 (1), 1–11 (Article number: 10973).

Gedzelman, S.D., Austin, S., Cermak, R., Stefano, N., Partridge, S., Quesenberry, S., Robinson, D.A., 2003. Mesoscale aspects of the urban heat island around New York City. Theor. Appl. Climatol. 75 (1–2), 29–42.

Grover, A., Singh, R., 2015. Analysis of urban heat island (UHI) in relation to normalized difference vegetation index (NDVI): a comparative study of Delhi and Mumbai. Environments 2 (2), 125–138.

Guha, S., Govil, H., Gill, N., Dey, A., 2020. A long-term seasonal analysis on the relationship between LST and NDBI using Landsat data. Quat. Res. (Pre-proof).

Jia, Y.Y., Tang, B., Zhang, X., Li, Z.L., July 23–27, 2007. Estimation of Land Surface Temperature and Emissivity from AMSR-E Data. Paper Presented at the Conference of Geoscience and Remote Sensing Symposium (IGARSS). Barcelona, Spain. Retrieved from: https://ieeexplore.ieee.org/stamp/stamp.jsp?tp=&arnumber=4423183.

Jordon, S.D., 2007. Global climate change triggered by global warming. Skeptical Inq. 31 (3), 32–39.

Kandlikar, M., Sagar, A., 1999. Climate change research and analysis in India: an integrated assessment of a South-North divide. Global Environ. Change 9 (2), 119–138.

Karoly, D.J., Braganza, K., Stott, P.A., Arblaster, J.M., Meehl, G.A., Broccoli, A.J., Dixon, K.W., 2003. Detection of a human influence on North American climate. Science 302 (5648), 1200–1203.

Keeling, C.D., 1997. Climate change and carbon dioxide: an introduction. Proc. Natl. Acad. Sci. USA 94 (16), 8273–8274.

Khandelwal, S., Goyal, R., Kaul, N., Mathew, A., 2018. Assessment of land surface temperature variation due to change in elevation of area surrounding Jaipur, India. Egypt. J. Remote Sens. Space Sci. 21 (1), 87–94.

Kimuku, C.W., Ngigi, M.M., 2017. Study of Urban heat island trends to aid in urban planning in Nakuru County-Kenya. J. Geogr. Inf. Syst. 9, 309–325.

Lal, D.S., 2017. Climatology (Revised Edition: 2017). Allahabad: Sharda Pustak Bhawan.

Li, Z.L., Becker, F., 1993. Feasibility of land surface temperature and emissivity determination from AVHRR data. Remote Sens. Environ. 43 (1), 67–85.

Li, Z.-L., Tang, B.-H., Wu, H., Ren, H., Yan, G., Wan, Z., et al., 2013. Satellite-derived land surface temperature: current status and perspectives. Remote Sens. Environ. 131, 14–37.

Liang, S., Shi, P., May 20–22, 2009. Analysis of the Relationship between Urban Heat Island and Vegetation Cover through Landsat ETM+: A Case Study of Shenyang. Paper Presented at 2009 Joint Urban Remote Sensing Event. Shanghai, China.

Mallick, J., Kant, Y., Bharath, B.D., 2008. Estimation of land surface temperature over Delhi using Landsat-7 ETM+. J. Ind. Geophys. Union 12 (3), 131–140.

Mannstein, H., 1987. Remote Sensing Applications in Meteorology and Climatology: Surface Energy Budget, Surface Temperature and Thermal Inertia. Springer, Dordrecht, pp. 391–410.

Mathew, A., Khandelwal, S., Kaul, N., 2016. Spatial and temporal variations of urban heat island effect and the effect of percentage impervious surface area and elevation on land surface temperature: study of Chandigarh city, India. Sustain. Cities Soc. 26, 264–277.

Mills, G., 2008. Luke howard and the climate of London. Weather 63 (6), 153–157.

Ministry of Statistics and Programme Implementation, Government of India, 2015. Statistics Related to Climate Change - India 2015. Retrieved from: http://www.mospi.gov.in/sites/default/files/publication_reports/climateChangeStat2015.pdf.

Mojolaoluwa, T.D., Emmanuel, O.E., Kazeem, A.I., 2018. Assessment of thermal response of variation in land surface around an urban area. Model. Earth Syst. Environ. 4 (2), 535–553.

More, R., Kale, N., Kataria, G., Rane, R.A., Deshpande, S., 2015. Study of the different approaches used to estimate the urban heat island effect in India. Int. J. Adv. Multidiscip. Sci. Emerg. Res. 4 (2).

Murata, A., Sasaki, H., Hanafusa, M., Kurihara, K., 2013. Estimation of urban heat island intensity using biases in surface air temperature simulated by a nonhydrostatic regional climate model. Theor. Appl. Climatol. 112 (1–2), 351–361.

Mustafa, E.K., Co, Y., Liu, G., Kaloop, M.R., Beshr, A.A., Zarzoura, F., Sadek, M., 2020. Study for predicting land surface temperature (LST) using landsat data: a comparison of four algorithms. Adv. Civ. Eng. 2020.

Mutiibwa, D., Kilic, A., Irmak, S., 2014. The effect of land cover/land use changes on the regional climate of the USA high plains. Climate 2 (3), 153–167.

NASA, 2018. Global Climate Change – Vital Signs of the Planet. Retrieved from: https://climate.nasa.gov/scientific-consensus/ (Accessed May 15, 2018).

Nimish, G., Bharath, H.A., Lalitha, A., 2020. Exploring temperature indices by deriving relationship between land surface temperature and urban landscape. Remote Sens. Appl. 18, 100299.

Oh, J.W., Ngarambe, J., Duhirwe, P.N., Yun, G.Y., Santamouris, M., 2020. Using deep-learning to forecast the magnitude and characteristics of urban heat island in Seoul Korea. Sci. Rep. 10 (1), 1–13.

Oke, T.R., 1982. The energetic basis of the urban heat island. Q. J. R. Meteorol. Soc. 108 (455), 1–24.

Oke, T.R., Cleugh, H.A., 1987. Urban heat storage derived as energy balance residuals. Boundary-Layer Meteorol. 39 (3), 233–245.

Pal, S., Ziaul, S., 2017. Detection of land use and land cover change and land surface temperature in English Bazar urban centre. Egypt. J. Remote Sen. Space Sci. 20 (1), 125–145.

Qian, Y., Wang, N., Li, K., Wu, H., Duan, S., Liu, Y., Li, C., 2020. Retrieval of surface temperature and emissivity from ground-based time-series thermal infrared data. IEEE J. Sel. Top. Appl. Earth Obs. Remote Sens. 13, 284–292.

Raloff, J., April 29, 1989. Global Smog: Newest Greenhouse Projection. Science News, pp. 262–263. Retrieved from. https://www.sciencenews.org/author/janet-raloff?sort_by=published_at&page=76 (Accessed 22 May 2019).

Ramachandra, T.V., Aithal, B.H., Sreekantha, S., 2012. Spatial metrics based landscape structure and dynamics assessment for an emerging Indian megalopolis. Int. J. Adv. Res. Artif. Intell. 1 (1), 48–57.

Ramachandra, T.V., Bharath, H.A., Vinay, S., Kumar, U., Venugopal, K.R., Joshi, N.V., 2016. Modelling and Visualization of Urban Trajectory in 4 Cities of India. Paper Presented at IISc-ISRO STC, Bangalore, India. Retrieved from: https://www.researchgate.net/publication/289687302_Modelling_and_Visualization_of_Urban_Trajectory_in_4_cities_of_India.

Ramachandra, T.V., Setturu, B., Nimish, G., Bhargavi, R.S., 2017. Monitoring Forest Dynamics within and Buffer Regions of Protected Areas in Karnataka, India (Sahyadri Conservation Series 63, ENVIS Technical Report 117. CES, Indian Institute of Science, Bangalore 560012. Retrieved from: http://wgbis.ces.iisc.ernet.in/biodiversity/sahyadri_enews/newsletter/Issue58/article1/SCR63_ETR117_National%20Parks_Karnataka.pdf.

Roth, M., 2012. Urban heat islands. In: Fernando, H.J.S. (Ed.), Handbook of Environmental Fluid Dynamics. Taylor and Francis, London, pp. 143−162.

Running, S.W., Justice, C.O., Salomonson, V., Hall, D., Barker, J., Carneggie, D., 1994. Terrestrial remote sensing science and algorithms planned for EOS/MODIS. Int. J. Remote Sens. 15 (17), 3587−3620.

Santra, A., 2019. Land surface temperature estimation and urban heat island detection: a remote sensing perspective. In: Santra, A., Mitra, S.S. (Eds.), Environmental Information Systems: Concepts, Methodologies, Tools, and Applications. IGI Global, USA, pp. 1538−1560.

Sarif, M., Rimal, B., Stork, N.E., 2020. Assessment of changes in land use/land cover and land surface temperatures and their impact on surface urban heat island phenomena in the Kathmandu valley (1988-2018). ISPRS Int. J. Geo-Inf. 9 (12), 726.

Schmugge, T.J., Becker, F., 1991. Remote sensing observations for the monitoring of land-surface fluxes and water budgets. In: Schmugge, T.J., André, J.C. (Eds.), Land Surface Evaporation. Springer, New York, USA, pp. 337−347.

Science for Environmental Policy, 2007. How Do Changes in Ocean Temperature Affect Marine Ecosystems? Retrieved from: http://ec.europa.eu/environment/integration/research/newsalert/pdf/52na2_en.pdf (Accessed 22 May 2019).

Scott, M.J., Rosenberg, N.J., Edmonds, J.A., Cushman, R.M., Darwin, R.F., et al., 1990. Consequences of climatic change for the human environment. Clim. Res. 1, 63−79.

Sismanidis, P., Keramitsoglou, I., Bechtel, B., Kiranoudis, C.T., 2016. Improving the downscaling of diurnal land surface temperatures using the annual cycle parameters as disaggregation kernels. Remote Sens. 9 (1), 23−42.

Sobrino, J.A., Jiménez-Muñoz, J.C., Zarco-Tejada, P.J., Sepulcre-Cantó, G., de Miguel, E., 2006. Land surface temperature derived from airborne hyperspectral scanner thermal infrared data. Remote Sens. Environ. 102 (1−2), 99−115.

Stewart, I.D., 2011. A systematic review and scientific critique of methodology in modern urban heat island literature. Int. J. Climatol. 31 (2), 200−217.

Stott, P.A., Mitchell, J.F., Allen, M.R., Delworth, T.L., Gregory, J.M., Meehl, G.A., Santer, B.D., 2006. Observational constraints on past attributable warming and predictions of future global warming. J. Clim. 19 (13), 3055−3069.

Tran, D.X., Pla, F., Latorre-Carmona, P., Myint, S.W., Caetano, M., Kieu, H.V., 2017. Characterizing the relationship between land use land cover change and land surface temperature. ISPRS J. Photogrammetry Remote Sens. 124, 119−132.

UN DESA, 2018. 2018 Revision of World Urbanization Prospects. Retrieved from: https://www.un.org/development/desa/publications/2018-revision-of-world-urbanization-prospects.html (Accessed 27 September 2018).

Wang, R., Murayama, Y., 2020. Geo-simulation of Land Use/cover Scenarios and Impacts on Land Surface Temperature in Sapporo, Japan. Sustain. Cities Soc. (Pre-proof).

Wolters, D., Brandsma, T., 2012. Estimating the urban heat island in residential areas in The Netherlands using observations by weather amateurs. J. Appl. Meteorol. Climatol. 51 (4), 711−721.

Yamashita, S., 1996. Detailed structure of heat island phenomena from moving observations from electric tramcars in metropolitan Tokyo. Atmos. Environ. 30 (3), 429−435.

Youneszadeh, S., Amiri, N., Pilesjo, P., 2015. The effect of land use change on land surface temperature in The Netherlands. Int. Arch. Photogram. Remote Sens. Spatial Inf. Sci. 40 (1), 745. https://dx.doi.org/10.5194/isprsarchives-XL-1-W5-745-2015.

Yu, X., Guo, X., Wu, Z., 2014. Land surface temperature retrieval from landsat 8 TIRS-comparison between radiative transfer equation-based method, split window algorithm and single channel method. Remote Sens. 6 (10), 9829−9852.

Global Urban Heat Island Mitigation

Global Urban Heat Island Mitigation provides a comprehensive picture of the global UHI microthermal interaction in different built environments. It explains the physical principles and how to moderate the undesirable consequences of swift and haphazard urban development to create more sustainable and resilient cities.

Global Urban Heat Island Mitigation provides extensive discussion on numerous UHI mitigation technologies and their effectiveness in cities around the globe. It proposes novel UHI mitigation technologies and strategies while assessing the effectiveness and suitability of UHI mitigation interventions in various climates and urban forms.

Key Features

- Adopts a multidisciplinary approach bridging theoretical and applied urban climatology with urban heat mitigation
- Compiles disparate urban climate research concepts and technologies into a coherent framework
- Includes contributions from leaders in fields from around the globe

About the Editors

Ansar Khan, Assistant Professor, Department of Geography, Lalbaba College, University of Calcutta, India

Hashem Akbari, Professor, Department of Building, Civil, and Environmental Engineering, Concordia University, Montreal, Quebec, Canada

Francesco Fiorito, Department of Civil, Environmental, Land, Building Engineering and Chemistry, Polytechnic University of Bari, Italy. Senior Visiting Fellow, University of New South Wales, Australia

Sk Mithun, Assistant Professor, Department of Geography, Haldia Government College, Vidyasagar University, India

Dev Niyogi, Dave P. Carelton Centennial Professor, Department of Geological Sciences, Jackson School of Geosciences and Department of Civil, Architectural, and Environmental Engineering, The University of Texas at Austin, Texas, USA

ELSEVIER elsevier.com/books-and-journals

ISBN 978-0-323-85539-6